Journal of Sciences, Islamic Republic of Iran 23(2): 147-161 (2012) http://jsciences.ut.ac.ir
University of Tehran, ISSN 1016-1104

Metamorphism of Late Neoproterozoic-Early Cambrian Schists in Southwest of Zanjan from the Soltanieh Belt in Northwest of Iran

A. Ghadimi, J. Izadyar,* S. Azimi, M. Mousavizadeh, and M. Eram

Department of Geology, Faculty of Science, Zanjan University Zanjan, Islamic Republic of Iran

Received: 6 February 2011 / Revised: 14 May 2012 / Accepted: 30 July 2012

Abstract

Late Neoproterozoic-Early Cambrian schists have been occurred in southwest of Zanjan city from the Soltanieh belt. The Soltanieh belt in northwest of Iran is uplifted basement of Precambrian-Paleozoic in main central Iran zone and includes outcrops of Precambrian, Paleozoic and Mesozoic Formations. Late Neoproterozoic-Early Cambrian schists, the oldest stratigraphy unit in the region, consist of phyllite, chlorite schist, mica schist and staurolite schist. Field and microstructural studies show several deformational phases in which the first phase (D_1) is well characterized by S_1 schistosity subparallel to the axial planes of F_1 fold. D_2 is a post D_1-phase of deformation recognized by kink-like mesoscopic folds that fold S_1 and the third phase (D_3) is characterized by strongly developed crenulation cleavage (S_3). Considering textural relationship, microstructural domain and mineral chemistry two main metamorphic events (M_1 and M_2) have been recognized. Geothermobarometry of the M_2 assemblage containing white mica, chlorite, biotite, plagioclase and quartz in the KNCMFASH system considering water saturated condition, yields pressure of 6.3Kbar and temperature of 690°C and the P-T estimates for the M_1 assemblage containing white mica, chlorite, biotite, plagioclase, staurolite and quartz yield pressure of 8.5Kbar and temperature of 580°C. The obtained clockwise P-T path shows an early intermediate pressure Barrovian type metamorphism (M_1) following by a low pressure Buchan type metamorphism (M_2). The deduced clockwise P-T path is characteristic of the metamorphic evolution of orogenic belts and probably originated through the convergence of the Gondwana and Eurasian plates during the Pan-African orogeny.

Keywords: Late Neoproterozoic-Early Cambrian schists; Soltanieh belt; Zanjan; Iran; Geothermobarometry

Introduction

Iranian crust constitutes one of the largest tectonic provinces in the southwestern Asia and is regarded as a complicated puzzle of continental fragments initially rifted from Gondwana which presently separated from each other by complex fold and thrust and discontinuous ophiolitic belts [5, 29]. The major tectonic provinces of

* Corresponding author, Tel.: +98(241)5154030, Fax: +98(241)5154002, E-mail: izadyar@znu.ac.ir

western and central Iran from north to south include: the Alborz mountains, a variety of small blocks composing central Iran, the Urmieh–Dokhtar arc, the Sanandaj–Sirjan zone, the Zagros mountains and the Zagros foreland (Arabian shield) [14] (Fig. 1). The major tectonic provinces are separated by two major suture zones representing closure of Paleotethys and Neotethys oceans. Paleotethys ocean closed during collision of Iran and Eurasia in the Late Triassic and Neotethys was closed in the Late Cretaceous or Tertiary because of collision of Arabia with Iran [3, 32, 33] (Fig. 1). Historically, intensely metamorphosed rocks (migmatite, gneiss, amphibolite and micaschist) that crop out in the major tectonic provinces of Iran (such as central Iran, Sanandaj-Sirjan, Alborz) visualized to present the Precambrian basement of the Iranian plateau [19, 34] and viewed as analogous of the Precambrian basement rocks exposed in the Arabian shield (e.g. [34]). It has been widely stated that the consolidation of the basement of Iranian plateau took place by the metamorphism and anatexis at about 11000 to 600 Ma [35,5,7]. However, earlier attempts at dating metamorphic rocks was controversial from Archean [13] to Early Proterozoic [27]. The earliest modern zircon U-Pb data include those of Samani et al. [26] for the Saghand (east central Iran) and Ozbak kuh (northern Lut block) area. Their U-Pb ages are mostly discordant and were interpreted to indicate magmatic and metasomatic events from Middle to Late Proterozoic. Ramezani [24] and Ramezani and Tucker [25] carried out the first extensive research on Iran basement complexes employing TIMS U-Pb zircon dating of a correlative suite of rocks in central Iran. They mentioned that the oldest documented and isotopically dated rocks in the Saghand region and probably the entire area of central Iran belong to the Tashk Formation with the depositional age between 627Ma and 533Ma. The well stratified sequence of weakly metamorphosed, sedimentary and volcanic/ volcaniclastic rocks that occur in vast area of Alborz, Zanjan, Azarbaijan is known as the Kahar Formation [8]. Crawford [6] was the first researcher who used Rb-Sr dating method for the Kahar Formation and obtained 645 Ma age. Horton et al. [17], using U-Pb age determination suggested a sediment source during Late Neoproterozoic-Early Cambrian sedimentation and proposed that deposition of the Kahar Formation was completed by the end of Early Cambrian in agreement with the Middle to Late Cambrian age assigned for overlying fossiliferous carbonate [11]. These data are in good agreement with a depositional age constrained between 627 Ma and 533 Ma for the Tashk Formation in central Iran, a lateral equivalent of the Kahar Formation [25]. Also, the possible correlatives for the Kahar Formation are successions including Morad series [18], Kalmard Formation [35] and upper Taknar Formation [23]. These imply that Kahar type facies is widely distributed throughout the Iranian plateau is likely underlie Phanerozic platform strata in many locations [25]. Although, these rocks are important to elucidate the geodynamic evolution of the Iranian plateau, but their metamorphic history have not hitherto been studied in detail. The studied metamorphic rocks are part of the Kahar Formation [36, 4] and provides the best opportunity to widen the existent knowledge of such rocks. Thus, the aims of this paper are: to present metamorphic data of Late Neoproterozoic-Early Cambrian schsits and also to clarify the geodynamic evolution of the region and to investigate the possible implications for metamorphic evolution of Kahar type rocks in the Iranian plateau.

Materials and Methods

1-Geological Setting

The Soltanieh belt forms a long and narrow

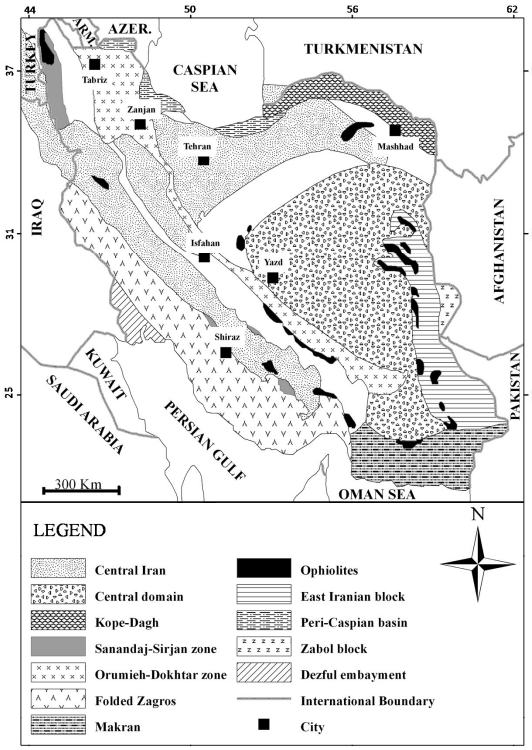

Figure 1. Major sedimentary and structural units of Iran (simplified from Aghanabati [1]).

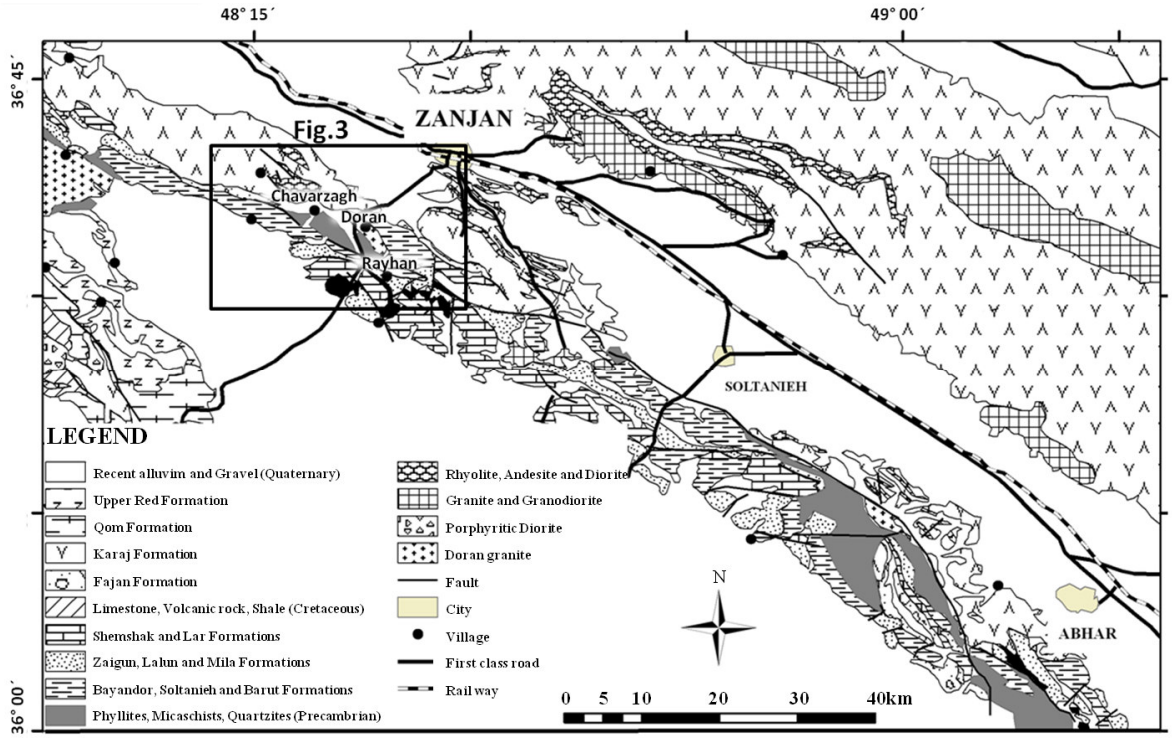

Figure 2. Geological map of the Soltanieh area (simplified from Stöcklin and Eftekharnezhad [36]).

northwest-southeast belt with more than 150 Km length and a maximum of 10 to 12 Km width [36]. The Soltanieh belt, in fact, is the uplifted basement of Precambrian-Paleozoic in main central Iran zone and maintains Precambrian, Paleozoic and even Mesozoic Formations completely similar to Alborz zone indicating that from Precambrian until the end of Jurassic, they formed one sedimentary basin [4]. This narrowness and the straight alignment of the uplift indicate it's nature as a major fault zone clearly expressed by a longitudinal fault along it's strike in northeast border (Fig. 2). Along the Soltanieh fault, the pre-Tertiary Formations of the Soltanieh belt are faulted against and partly thrust over the Tertiary Formations which fill the Zanjan-Abhar depression (Fig. 2). In contrast to the faulted northeast border the southwest border in spite of its straight alignment gives no surface evidence of faulting. The straight alignment of the southwestern mountain border may thus be explained as a surface expression of persistent line of down-flexuring below the southwest plain of Kavand-Do Tappeh (Fig. 2). In additional to the bordering thrust fault in the northeast and border flexture in the southwest, both having straight northwest-southeast trend, the Soltanieh mountains display a great number of cross faults of various directions that disrupt the pre-Tertiary Formations into a complicated mosaic-like fault block pattern [36, 4] (Fig. 2). Complete sequence of detritic, pyroclastic and carbonate thick deposits (Kahar, Bayandor, Soltanieh, Barout and Lalun Formations) are present in the study area which are important for the geological analysis of the Iranian crust [36] (Figs. 2 and 3). Interestingly, the type localities of Bayandor, Soltanieh and Barout Formations have been selected from within the study area [36]. Horton et al. [17] present TIMS zircon U-Pb results for the mentioned sequence. Their zircon U-Pb data show that earliest sediment accumulation commenced in the Latest Neoproterozoic prior to the Precambrian-Cambrian boundary. The Late Neoproterozoic-Early Cambrian age of Kahar, Bayandor, Soltanieh, Barout and Lalun Formations was also assigned by other researchers (e.g. [34, 35, 5, 27, 2]). Considering these studies, in this paper, this sequence was also considered as Late Neoproterozoice-Early Cambrian deposits. From the southwest of Zanjan and in contact with Doran granite from south of Chavarzagh village towards north of Rayhan village, a metamorphic complex with NW-SE

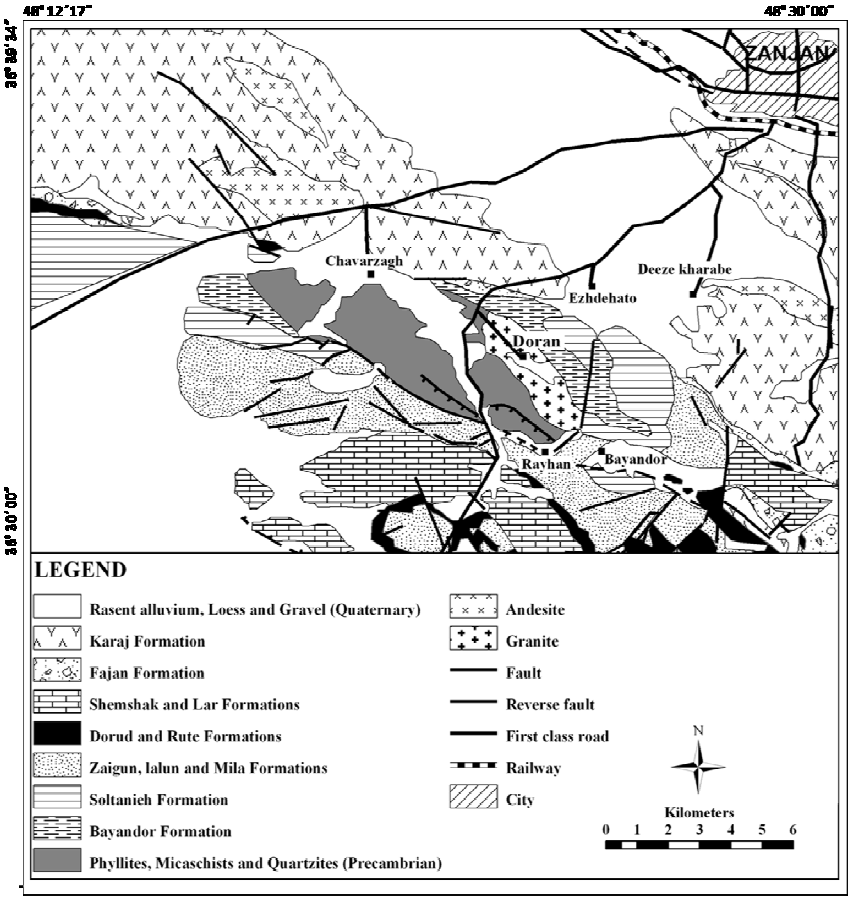

Figure 3. Geological map of the studied area (simplified from Babakhani and Sadeghi [4]).

trend has been outcropped (Fig. 3). It consists of phyllite, chlorite schist, mica schist and staurolite schist with lenses and layers of quartzite and talc schist. They have been considered as the oldest stratigraphic unit in the area [36, 4]. The metamorphic complex cannot be sharply separated from the barely metamorphosed slate sequences constituting the Kahar Formation but seems to be linked with them by both vertical and lateral transitions [36]. Thus, it is possible to consider them as a lateral equivalent of the Kahar Formation which differ because of different metamorphic grade so that from Chavarzagh village towards Rayhan village, metamorphic mineral zones including chlorite, biotite and staurolite can be determined. In the study area, Ordovician, Silurian and Devonian deposits have not been observed and the Permian deposits (Dorud and Ruteh Formations) overly uncomformably the Milla Formation (Figs. 2 and 3). Such observation was also reported by other researchers (e.g. [36, 4]). Mesozoic deposits contain detrital deposits of the Shemshak Formation and limestones of the Lar Formation (Figs. 2 and 3). The Shemshak Formation deposits include a sequence of shale with sandstone interlayers and occasionally thin lenticular layers of coal. On the basis of fossil plants, the Rhaeto-Liassic age has been considered for the Shemshak Formation [36, 4]. In the Soltanieh mountain, the soft-weathering shales and sandstones of the Shemshak Formation are conformably overlain by limestone of the Lar Formation. Tertiary deposits consist of a sequence of detrital, pyroclastic and volcanic rocks which are equivalent to the Karaj Formation in Alborz. The overlap of the Tertiary deposits on older Formations is with unconformity everywhere, which begins with Fajan conglomerate [36] (Figs. 2 and 3). In the study area, the contact between the Fajan and older units is faulted. This observation appears to be supported by the fact that Fajan conglomerate do not contain any clasts of the

metamorphic complexes. This observation was also supported by other researchers (e.g. [14]). A small body of deeply eroded leucogrnite is partially exposed in the low topography around the village of Doran, about 12 Km south of Zanjan. Stöcklin and Eftekharnezhad [36] mapped this intrusion as the Doran granite (Figs. 2 and 3). The leucogranite contact with the Bayandor and Fajan Formations is faulted [14] but it is intruded into the Kahar Formation and the metamorphic complex and locally caused generation of biotite hornfels in the contact aureole. Within Doran leucogranite, large enclaves of slate and phyllite of the Kahar Formation and metamorphic complex could be seen. Stöcklin and Eftekharnezhad [36] asserted that the siliciclastic Neoproterozoic Bayandor Formation unconformably overlies the eroded and saprolitic surface of the granite. Based on this relationship, Doran granite has been considered in the literature as the type example of Precambrian plutonism in Iran [14]. Hassanzadeh et al. [14] by using TIMS zircon U-Pb geochronology found two astonishingly different age for Doran granite (2.8 ± 0.1Ma and 567 ± 19Ma). Using cathodoluminescence

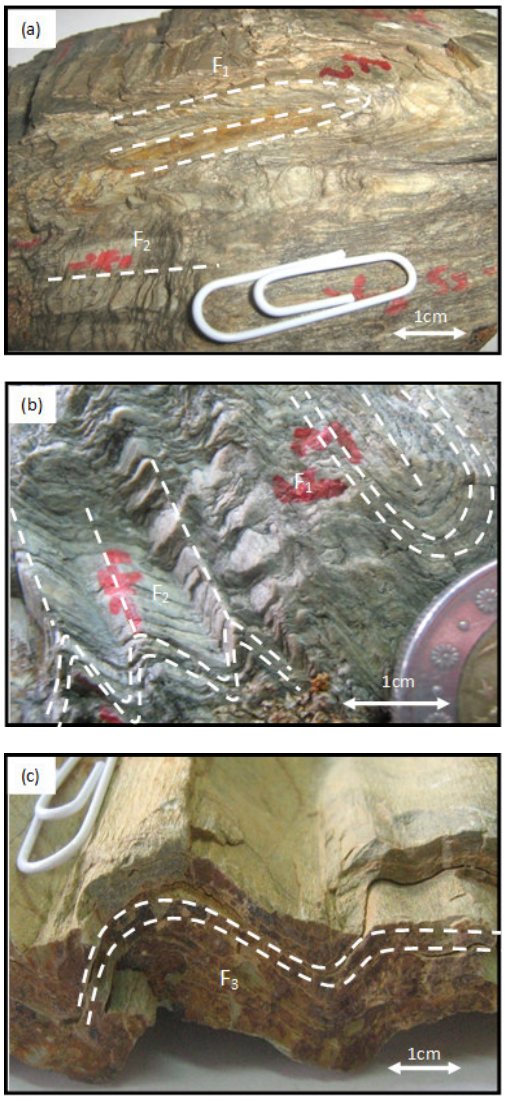

Figure 4. Photograph of biotite-chlorite-muscovite schist showing a) F_1 and F_2 folds b) F_1 and F_2 folds c) F_3 fold.

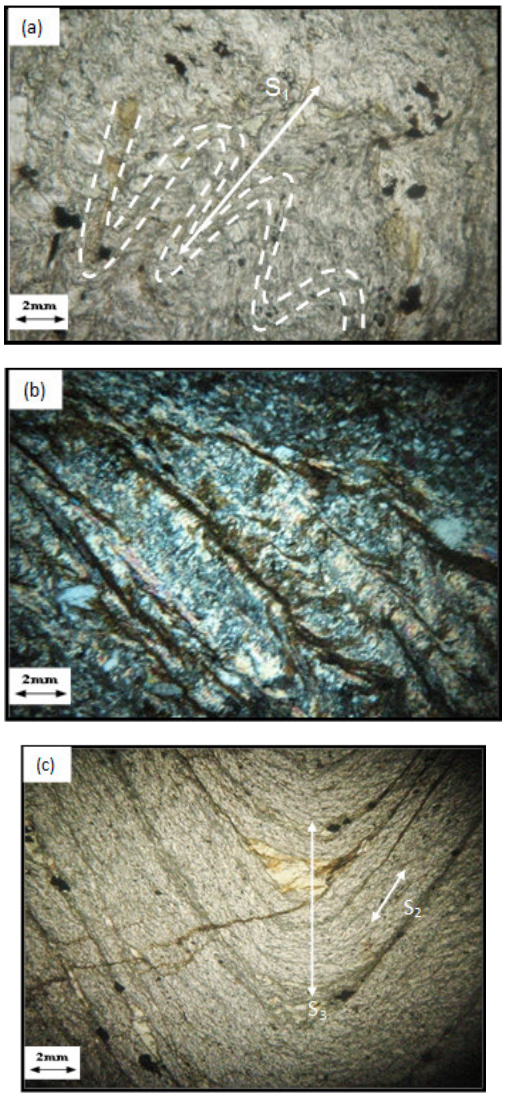

Figure 5. Photomicrograph of biotite-chlorite-muscovite schist showing a) S_1 schistosity b) S_2 schistosity c) S_2 and S_3 schistosities.

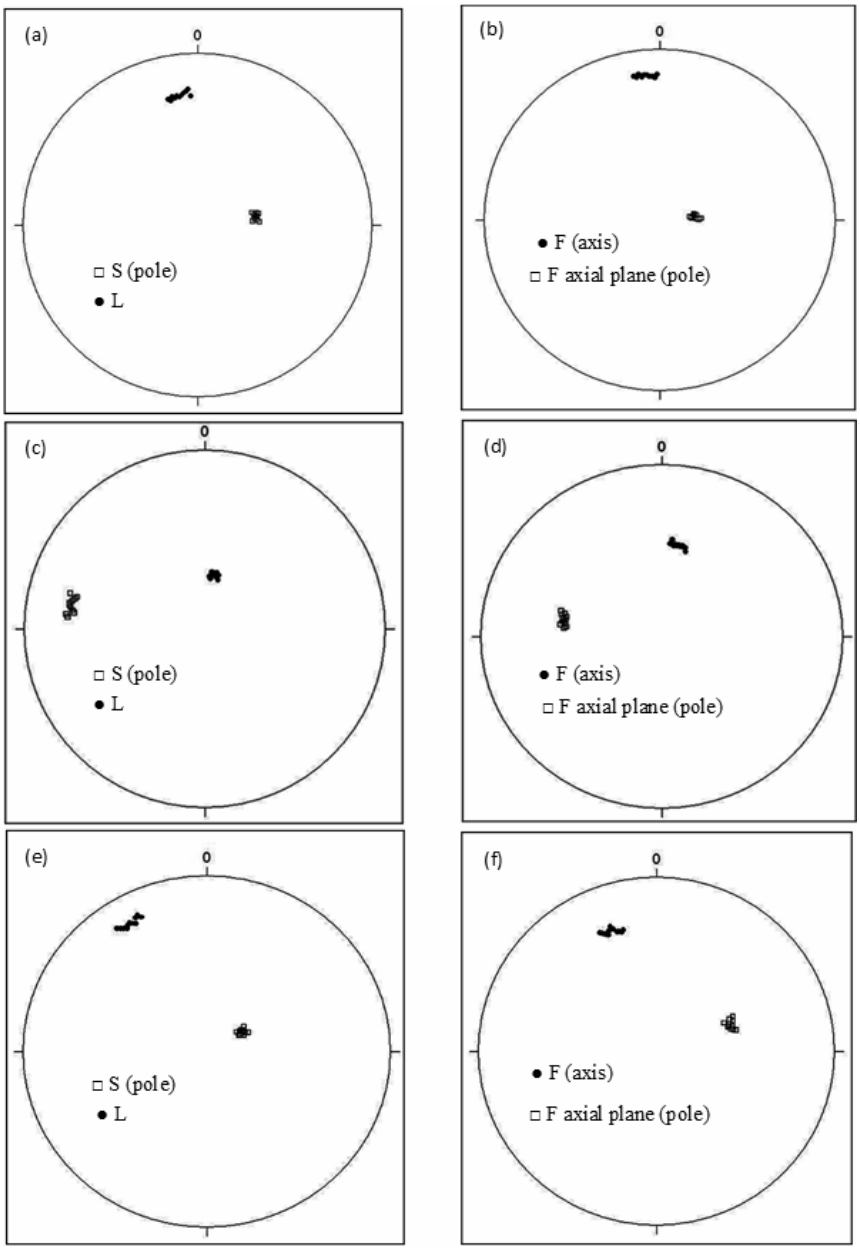

Figure 6. Mesoscopic orientation data for a) S_1 schistosity and L_1 lineation b) F_1 fold c) S_2 schistosity and L_2 lineation d) F_2 fold e) S_3 schistosity and L_3 lineation f) F_3 Fold.

method, they revealed the inherited cores in some of the zircons. Considering similar granite in Soltanieh belt such as Sarvejahan and Moghanlou, they believe to the existence of Neoproterozoic plutonism [14].

2-Deformational Phases

The main study area is along a northwest-southeast traverse stretching from Chavarzagh village towards the Rayhan village (Fig. 3). Field studies have focused on mesoscopic structures and several discrete deformation stages are recognized.

2-1- D1 Deformation

The main structures formed during deformation stage of D_1 are a S_1 schistosity and associated stretching

lineation (L_1) (Figs. 4a, 4b and 5a). The main L_1 forming minerals are chlorite and muscovite, which are aligned on the S_1 plane (Fig. 5a). S_1 and L_1 are dominant in the northwestern part of the study area. The orientation data of S_1 and L_1 are plotted in Figure 6a. Mesoscopic folds formed during D_1 (shown as F_1) are dominantly found in the northwestern part of the study area. F_1 folds are generally tight with an orientation trend as shown in Figure 6b. These folds are regarded to be formed during D_1 because: (i) the folds have flat lying axial planes and N-S trending axes, and the orientations of these structures are the same as those of S_1 and L_1 (Figs. 6a and 6b) and (ii) a newly formed schistosity (S_1) is commonly observed subparallel to the axial planes of the folds and stretching lineation parallel to the fold axes (Figs. 4a, 4b and 5a). It is widely recognized irrespective of the original orientation that folds associated with high strain will tend to have their axes parallel to the maximum finite stretching direction and their axial planes will be parallel to the new schistosity (e.g. [40]).

2-2- D2 Deformation

D_2 is a post-D_1 phase of deformation recognized most readily by kink-like mesoscopic folds that fold S_1 (Figs. 4a and 4b). This type of fold, generally on a centimeter scale is termed F_2. In this area, most of the F_2 crenulations (with wavelength about 1 Cm) on the S_1 plane are oblique to L_1 and L_1 is clearly folded by F_2 crenulation (Figs. 4a and 4b). The orientation data of F_2, S_2 and L_2 are plotted in Figures 6c and 6d and show that the orientation data of F_2 are the same as those for S_2 and L_2 structures, therefore it can be inferred that both were formed during D_2 deformation. Chlorite, muscovite, biotite and staurolite are mostly found in the limbs while quartz and albite can be recognized in the hinges of crenulations (Fig. 5b).

2-3- D3 Deformation

The main structures formed during this deformation are strongly developed crenulation cleavage (S_3) and associated stretching lineation (L_3) (Fig. 4c). The main L_3 forming minerals are biotite, chlorite and muscovite and their alignment on the S_3 plane can be observed (Fig. 5c). This deformation produce the dominant structures in the study area and developed by folding the previous foliations. Although the effect of the D_3 can be recognized in all of the study area but dominantly can be seen in southeastern part which diminished other traces of older deformations. Mesoscopic to macroscopic folds formed during D_3 (shown as F_3) are also frequently found in the southeastern part with an orientation shown in Figure 6f. The orientation data show that newly formed schistosity (S_3) is commonly observed subparallel to the axial planes of folds and the related stretching lineation parallel to the fold axes (Figs. 6f and 6e). S_3 and L_3 were defined by biotite, muscovite and chlorite crystals oriented parallel to the axes of the crenulations (Fig. 5c). Sometimes S_3 is identified by spaced foliation defined by mica-rich bands and quartz-feldspar bands both in mesoscopic and microscopic scales.

3- Petrography

From northwest (Chavarzagh village) towards southeast (Rayhan village) of the study area, three mineral zones by increasing metamorphic grade have been recognized.

Chlorite zone: Rocks of the chlorite zone are phyllite, chlorite schist, and muscovite chlorite schist. Mineral assemblage of this zone consists of quartz, muscovite, chlorite, albite ± orthoclase (Table 1).

Biotite zone: The main observed metamorphic rocks of the study area belong to the biotite zone. The main rock type of this zone includes muscovite-chlorite-biotite schist. Mineral assemblage of the biotite zone contains biotite, albite, chlorite, quartz, muscovite ± orthoclase. (Table 1).

Staurolite zone: The first occurrence of staurolite is in the staurolite schist near the Rayhan village in SE of the study area. The mineral assemblage of staurolite schist is staurolite, biotite, muscovite, chlorite, plagioclase and quartz (Table 1). Other metamorphic rocks such as talc schist and quartzite are also observed as intercalations within pelitic schist.

Muscovite is present in all of the rocks examined but its size, modal percentage and chemical composition vary from chlorite to staurolite zones and also in different textural domains. In the chlorite zone, fine grain (usually less than 0.1mm) muscovite can be found within slaty cleavage which it can be termed sercitie instead of muscovite. But in biotite and staurolite zones, muscovite up to 0.3mm long has developed in the rocks. Its modal percentage decreases with increasing metamorphic grade. Muscovite is a major constituent mineral of D_1, D_2 and D_3 phases of deformations, forming L_1 alignment on the S_1 plane and L_2 on the limbs of F_2 crenulation and L_3 associated stretching lineation developed in D_3.

Chlorite is present in all of the examined rocks but is a major constituent minerals especially in the rocks of the chlorite and biotite zones. It is also occurred in different textural domains. In the chlorite zone, it is usually less than 0.1mm in size and is recognized in the slaty cleavage of the constituent rocks of this zone but

Table 1. Parageneses of the main studied samples. (+) and (-) indicate presence or absence of the minerals respectively

Sample No.	SZ42	SZ41	BZ23	BZ22	BZ21	CZ13	CZ12	CZ 10
Muscovite	+	+	+	+	+	+	+	+
Chlorite	+	+	+	+	+	+	+	+
Biotite	+	+	+	+	+	−	−	−
Staurolite	+	+	−	−	−	−	−	−
Albite	+	+	+	+	+	+	+	+
Quartz	+	+	+	+	+	+	+	+
Alkalifeldspar	−	−	−	−	−	+	+	+

Table 2. Representative analyses of the main mineral groups

Mineral name	Staurolite	Albite			Chlorite			Biotite			Muscovite		
Metamorphic zone	St	St	Bt	Bt	St	Bt	Bt	St	Bt	Bt	St	Bt	Bt
Deformation phase	D_3	D_3	D_3	D_2	D_3	D_3	D_2	D_3	D_3	D_2	D_3	D_3	D_2
Sample No	SZ42	SZ42	BZ23	BZ22	SZ42	BZ23	BZ22	SZ42	BZ23	BZ22	SZ42	BZ23	BZ22
Point No	221	220	112	111	211	102	101	215	103	107	210	109	105
SiO_2	25.06	63.3	64.01	65.93	26.11	26	25.37	34.4	33.82	34.7	46.82	49.01	50.12
TiO_2	0.2	-	-	-	0.33	0.3	0.2	1.01	1.9	1.03	0.2	0.15	0.1
Al_2O_3	54.62	24	22.2	21.62	23.12	25.01	24.12	19.21	19.62	18.52	34.8	33.21	32.19
FeO	13.84	-	-	-	24.22	19.02	21.02	21.04	19.7	22.4	1.14	1.04	0.89
MgO	1.41	-	-	-	14.67	18.01	17.51	10.61	8.21	6.83	0.48	0.51	0.71
CaO	0.2	3.01	2.12	1.12	0.01	0.03	0.02	0.1	0.1	0.1	0.04	0.03	0.05
Na_2O	0.1	9.5	10.9	11.5	-	-	-	0.1	0.12	0.1	0.1	0.2	0.18
K_2O	-	0.07	0.08	0.1	0.05	0.05	0.06	9.12	9.01	8.89	8.85	8.5	8.23
Total	95.43	99.88	99.31	100.3	88.51	88.42	88.3	95.59	92.48	92.58	92.43	92.66	92.48
	O=22		O=8			O=14			O=11	O=11		O=11	
Si	7.16	2.794	2.842	2.907	2.692	2.637	2.584	2.614	2.666	2.756	3.16	3.28	3.349
Ti	0.043	-	-	-	0.026	0.02	0.015	0.058	0.11	0.062	0.01	0.008	0.005
Al^{tet}	-	1.248	1.162	1.093	1.308	1.362	1.416	1.386	1.334	1.244	0.84	0.72	0.651
Al^{oct}	18.4	-	-	-	1.503	1.627	1.481	0.335	0.486	0.49	1.929	1.9	1.885
Fe^{2+}	3.307	-	-	-	2.089	1.613	1.791	1.118	1.298	1.488	0.052	0.06	0.05
Fe^{3+}	-	-	-	-	-	-	-	0.197	-	-	0.011	-	-
Mg	0.6	-	-	-	2.255	2.725	2.658	1.202	0.947	0.808	0.048	0.05	0.071
Ca	0.061	0.142	0.101	0.053	0.001	0.003	0.002	0.008	0.009	0.009	0.003	0.002	0.004
Na	0.055	0.811	0.938	0.983	-	-	-	0.015	0.02	0.015	0.013	0.03	0.023
K	-	0.002	0.005	0.006	0.007	0.006	0.008	0.885	0.9	0.902	0.763	0.73	0.702
Total	29.62	4.997	5.048	5.042	9.881	9.993	9.955	7.818	7.77	7.774	6.829	6.78	6.740
X_{mu}	-	-	-	-	-	-	-	-	-	-	0.84	0.72	0.651
X_{cel}	-	-	-	-	-	-	-	-	-	-	0.048	0.05	0.071
X_{phl}	-	-	-	-	-	-	-	0.4	0.312	0.269	-	-	-
X_{ann}	-	-	-	-	-	-	-	0.4	0.2	0.241	-	-	-
X_{ames}	-	-	-	-	0.44	0.391	0.334	-	-	-	-	-	-
X_{clin}	-	-	-	-	0.275	0.341	0.368	-	-	-	-	-	-
X_{ab}	-	0.811	0.938	0.983	-	-	-	-	-	-	-	-	-
X_{an}	-	0.187	0.057	0.011	-	-	-	-	-	-	-	-	-

in the biotite zone it occasionally reaches up to 0.5mm long can be seen as alignted parallel to the S_3 schistosity. It's modal percentage decreases towards the staurolite zone and in this zone it is minor constituent minerals. Chlorite is also present in D_1, D_2 and D_3 phases of deformation.

Biotite was found in pelitic schists of the biotite and staurolite zones and it is one of the major constituent minerals of these zones. It is also occurred in two microstructural domains of D_2 and D_3.

Albite is present in the rocks of chlorite, biotite and staurolite zones. It's size and chemical composition changes with increasing grade of metamorphism from chlorite zone towards the staurolite zone. In the chlorite zone it is usually very fine and is very difficult to distinguish it from quartz. Albite is also occurred in two microstructural domains of D_2 and D_3.

4- Mineral Chemistry

Mineral analysis was preformed with a Cameca SX100 electron probe microanalyzer (10 KV, 10 nA) using albite (Na), orthoclase (Al, K), anorthite (Ca), diopside (Mg, Si), $MnTiO_3$ (Mn, Ti) and Fe_2O_3 (Fe) as standards in KMA research group in Malaysia. The structural formulae, the Fe^{3+}-iron and end-member activities of the minerals were recalculated with the Ax program of Holland and Powell (www.esc.com.ac.uk/ pub/minp/AX). Mineral abbreviations are from Holland and Powell [16].

4-1- Muscovite

Muscovite analyses are listed in Table 2. The number of cations is calculated on the basis of 11 oxygens. The main constituent end-member is muscovite and celladonite and paragonite being the other end-members. Comparison of the muscovite compositions from the biotite and staurolite zones shows that muscovite in staurolite zone contains more muscovite end-member (biotite zone muscovite composition: $X_{mu} = 0.718$, $X_{cel} = 0.051$; staurolite zone muscovite composition: $X_{mu} = 0.84$, $X_{cel} = 0.048$) (Table 2). Reduction in the phengite substitution of muscovite with metamorphic grade has been described by several authors in different low to medium pressure metamorphic terrains [39, 9]. There are no distinct compositional differences between those lying parallel to the S_1 schistosity and those oblique to S_1 on S_2 schistosity. Muscovite of D_3 deformation is richer in muscovite end-member and slightly depleted in celladonite component (D_2-muscovite composition: $X_{mu} = 0.651$, $X_{cel} = 0.07$; D_3-muscovite composition: $X_{mu} = 0.718$, $X_{cel} = 0.051$) (Table 2).

4-2- Chlorite

Representative analyses of chlorite are tabulated in Table 2. The number of cations is calculated on the basis of 14 oxygen. According to Table 2, chlorite is composed of two main end-members of clinochlore and amesite. The mole fractions of other component are negligible. Comparing the chemical composition of chlorite from the biotite and staurolite zones, it can be inferred that with increasing metamorphic grade from the biotite zone towards staurolite zone, the amesite component of chlorite increases while clinochlore component decreases (biotite zone chlorite composition: $X_{ames} = 0.391$, $X_{clin} = 0.341$; Staurolite zone chlorite composition: $X_{ames} = 0.44$, $X_{clin} = 0.275$ (Table 2). Regarding differences of chemical compositions between chlorite lying parallel to the S_1 and S_2, distinct compositional differences cannot be observed. Comparing chemical compositions of chlorites formed during D_2 and D_3 deformations show that D_2-chlorite is richer in clinochlore and poorer in amesite end-members (D_2-chlorite composition: $X_{clin} = 0.368$, $X_{ames} = 0.334$; D_3-chlorite composition: $X_{clin} = 0.341$, $X_{ames} = 0.391$). (Table 2, Fig. 7b).

4-3- Biotite

Microprobe analyses of biotite are provided in Table 2. The number of cations is calculated on the basis of 11 oxygen. On the average, the phlogopite and annite end-members made up to 60 percentage of biotite composition and the remaining is mostly eastonite component (Table 2). From the biotite zone towards the staurolite zone, the phlogopite end-member increases (biotite zone biotite composition: $X_{phl} = 0.312$, $X_{ann} = 0.20$; staurolite zone biotite composition: $X_{phl} = 0.4$,

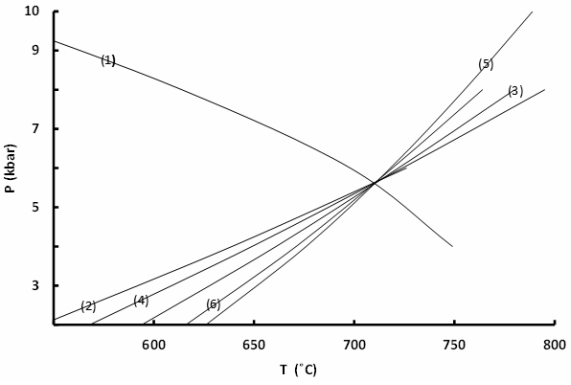

Figure 7. Stable intersection involving muscovite, paragonite, clinochlore, phlogopite, eastonite, albite, quartz and H_2O for M_2 assemblage.

Table 3. The stability periods for minerals and the relationship between metamorphism, mineral crystallization, mineral composition and deformational phases

Mineral name	Deformational Phases: D_1 / D_2 / D_3 — Metamorphic stages: M_1 / M_1 / M_2	Microstructural domains	Mineral compositin
Muscovite	———	L_1 alignment on the S_1 plane	X_{mu}=0.651 , X_{cel}=0.07
Muscovite	———	Limbs of F_2 crenulation	X_{mu}=0.651 , X_{cel}=0.07
Muscovite	———	L_3 stretching lineation on S_3 plane	X_{mu}=0.718 , X_{cel}=0.051
Chlorite	———	L_1 alignment on the S_1 plane	X_{clin}=0.368 , X_{ames}=0.334
Chlorite	———	Limbs of F_2 crenulation	X_{clin}=0.368 , X_{ames}=0.334
Chlorite	———	L_3 stretching lineation on S_3 plane	X_{clin}=0.341 , X_{ames}=0.391
Biotite	———	Limbs of F_2 crenulation	X_{phl}=0.269 , X_{ann}=0.241
Biotite	———	L_3 stretching lineation on S_3 plane	X_{phl}=0.312 , X_{ann}=0.20
Staurolite	———	Limbs of F_2 crenulation	Fe-Mg Staurolite
Albite	———	Hinges of F_2 crenulation	X_{ab}=0.983 , X_{an}=0.011
Albite	———	L_3 stretching lineation on S_3 plane	X_{ab}=0.983 , X_{an}=0.057
Quartz	———		

X_{ann} = 0.4). Biotite from D_3 deformation contains more phlogopite and slightly less annite end–member (D_2–biotite composition: X_{phl} = 0.269, X_{ann} = 0.241; D_3-biotite composition: X_{phl} = 0.312, X_{ann} = 0.20) (Table 2).

4-4- Albite

The major constituent end-member of albite is albite and anorthite being the second constituent (Table 2). It's chemical composition changes from the biotite zone towards the staurolite zone in which it becomes richer in anorthite and poorer in albite end-members (Chemical composition of albite from biotite zone: X_{ab} = 0.938, X_{an} = 0.057; chemical composition of albite from staurolite zone: X_{ab} = 0.811, X_{an} = 0.187) (Table 2). Also, clear differences between albite in S_3 schistosity and those of S_2 schistosity can be seen. Albite forming in D_3 deformation is richer in anorthite and poorer in albite components (chemical composition of albite of D_3-deformation: X_{ab}=0.938, X_{an}=0.057; chemical composition of albite of D_2-deformation: X_{ab}=0.983, X_{an}=0.011) (Table 2).

4-5- Staurolite

Staurolite is a porphyroblast phase and only occurs in staurolite zone in the southeast of the area where only S_2 schistosity can be seen. Commonly it is euhedral and chemically homogenous. The average chemical composition of staurolite is tabulated in Table 2.

5- Thermobarometry

Considering the relationship between deformational

Table 4. 6 stable reactions (a) and 4 independent set of reactions (b) obtained for M_2 assemblage containing white mica, chlorite, biotite, plagioclase, quartz and fluid phases in the K_2O-Al_2O_3–SiO_2–MgO–FeO–Na_2O–CaO–H_2O (KNCMFASH) system

a)
[1] 5mu+3clin+8ab = 8pa+5phl+9q+4H_2O
[2] 14pa+11phl = 2mu+3clin+9east+14ab+2H_2O
[3] 6pa+5phl = clin+5east+6ab+2q+2H_2O
[4] mu+2pa+2phl = 3east+2ab+3q+2H_2O
[5] 3mu+clin+phl = 4east+7q+4H_2O
[6] 5mu+2clin+2ab = 2pa+5east+11q+6H_2O
b)
[7] Clin+east = ames+phl
[8] 2pa+3cel = 2mu+phl+2ab+2H_2O+3q
[9] 14pa+9ames+20ann=2mu+12daph+18east+14ab+2H_2O
[10]8pa+7ames+15ann+2q = 2cel+9daph+13east+8ab

phases, microstructural domains and mineral compositions, two metamorphic stages can be recognized: (1) a higher pressure metamorphic event (M_1) that is produced during the D_1 and (2) a lower pressure and higher temperature metamorphism (M_2) that has resulted from D_3 episode of deformation (Table 3). D_1 recognized by a S_1 schistosity and associated stretching lineation (L_1) produced by generally tight folds of F_1 and D_2 recognized by a S_2 and L_2 structures originated by F_2 crenulation. Altough D_1 and D_2 are vividly two different deformational phases but their mineral compositions are similar, therefore, they have been attributed to a single metamorphic stage of M_1 (Table 3). The first metamorphic stage (M_1) is characterized by mineral assemblage of muscovite, chlorite, biotite, staurolite and quartz forming the S_1 and S_2 schistosities. The second metamorphic stage (M2) can be recognized by mineral assemblage like muscovite, chlorite, biotite, albite and quartz forming L_3 on the S_3 plane that produced during D_3 episode of deformational phase.

Selected minerals involved in the same microstructural domain and in close contact are regarded to have crystallized coevally in thermo-dynamic equilibrium. For calculations, we used the internally consistent thermodynamic data set of Holland and Powel [16] and the program TERMOCALC V3.21 [15, 16]. Accuracy on the P-T estimates, estimated by the error ellipse parameters is typically of the order of 10-30°C for temperature and 1-2kbars for pressure. Some end-members presented only in small amounts such as magnesio-staurolite for staurolite which produce a large uncertainty on the results were removed but in some cases such as daphinite in chlorite was not omitted because of its importance for finding metamorphic reactions. Pressures and temperatures during metamorphism were estimated using crossing reactions curves of independent reactions obtained from average P-T mode incorporated in TERMOCALC V3.21. To ensure that the estimated P-T is not an artifact, stable invariant points and univariant reactions were obtained using Schreinemakers' analysis. The P-T positions of the invariant point and univariant equilibria have been determined using THERMOCALC V3.2.1. For the construction, the fluid phase was assumed to be in excess and water activity was assumed to be 1.0 as already inferred from the observed metamorphic assemblage. For M_2 assemblage, containing white mica, chlorite, biotite, plagioclase, quartz and water, the system K_2O-Al_2O_3–SiO_2–MgO–FeO–Na_2O–CaO–H_2O (KNCMFASH) with phase components including muscovite, paragonite, celladonite, clinochlore, daphinite, amesite, phlogopite, annite, eastonite, albite, anorthite, quartz and H_2O was considered. Doing Schreinemakers' analysis for the system gives 31 univariant reactions and 11 intersections in which only one intersection is stable (Fig. 7). The stable intersection involving muscovite, paragonite, clinochlore,

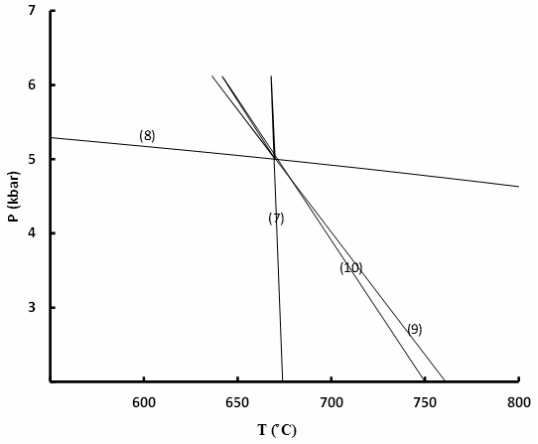

Figure 8. Cross cutting of independent reactions for M_2 assemblage.

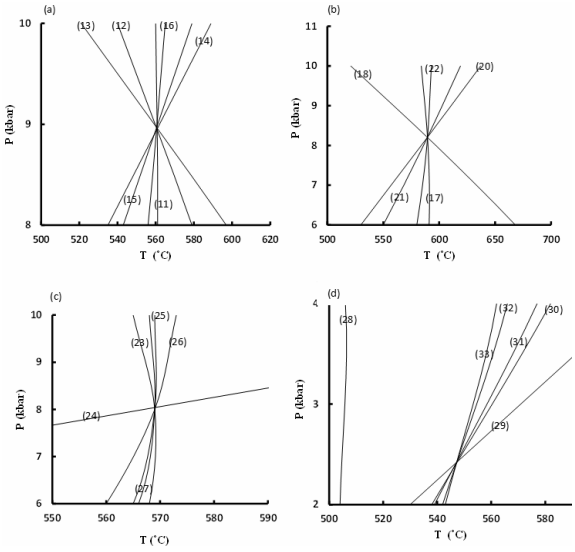

Figure 9. Stable intersections for M_1 assemblage containing phases of white mica, chlorite, biotite, plagioclase, staurolite, quartz and fluid. a) Stable intersection containing mu, cel, clin, daph, ann, fst, q and H_2O. b) Stable intersection containing mu, cel, clin, phl, ann, fst, q and H_2O. c) Stable intersection containing mu, clin, ames, phl, ann, east, fst, and H_2o d) Stable intersection containing mu, clin, ames, phl, ann, east, fst and H_2O.

phlogopite, eastonite, albite, quartz and H_2O or [cel, ames, daph, ann] contains 6 stable reactions (Fig. 7) (Table 4a). An invariant point (at P=5.6kbar, T=710°C) (Fig. 7) has been calculated for the mentioned system, in which activities of the phases adjusted for one as a model system. Independent set of reactions has been calculated using average P-T mode in THERMOCALC (Table 4b) (Fig. 8). They cross cut aaround 5kbar and 670°C (Fig. 8). Both calculations vividly show that the first stage of metamorphism was high-temperature and relatively low pressure.

M_1 assemblage contains phases of white mica, chlorite, biotite, plagioclase, staurolite, quartz and water in the system of K_2O–Al_2O_3–SiO_2–MgO-FeO-Na_2O–CaO–H_2O (KNCMFASH) with end-member components including muscovite, paragonite, celladonite, clinochlore ,daphinite, amesite, phlogopite, annite, eastonite, Fe-staurolite, albite, anorthite, quartz and H_2O. Clearly, the chemical compositions and modal percentages of the M_2-stage differ from M_1-stage. Schrinemakers' analysis of the system indicates four stable intersections which except one of them cross cut at P=8-9kbar, T=561-589°C (Fig. 9). They include stable intersections [pa, ames, phl, east, ab] involving muscovite, celladonite, clinochlore, daphinite, annite, Fe-staurolite, quartz, H_2O; [pa, ames, daph, east, ab] involving muscovite, celladonite, clinochlore, phlogopite, annite, Fe-staurolite, quartz, H_2O; [pa, cel, daph, ab, q] involving muscovite, annite, eastonite, Fe-staurolite, H_2O and [pa, cel, ames, daph, ab] involving muscovite, clinochlore, phlogopite, annite, eastonite, Fe-staurolite, quartz, H_2O (Fig. 9, Table 5a,b,c,d). Independent set of reactions obtained from average P-T calculation in THERMOCALC gives an average temperature of 600°C and pressure of 8kbar pressure (Fig. 10) (Table 5e).

Results and Discussion

The commonly accepted Neoproterozoic paleogeographic reconstruction of the continents, place the Iranian terranes along the Paleotethyan margin of Gondwana supercontinent between the Zagros margin of Arabia and northwestern margin of the Indian plate (e.g. [33, 25, 14]). It usually discussed that the Late Neoproterozoic-Early Cambrian magmatism and sedimentation in Iran is the result of crustal extension associated with continental drift which was accompanied by emplacement of alkaline magmatism [5,27,2]. It is believed that the vast carbonate-evaporate deposits of the Zagros mountains (Hormuz Formation) and their correlative rocks in the region (e.g. Salt Range in Pakistan) are deposited in the rift basins associated with the post-collisional, transcurrent faults produced after the Pan-African orogeny [5,20]. On the other hand, Talbot and Alavi [37] proposed an aborted rift tectonic model involving Late Neoproterozoic-Early Cambrian crust that underwent extension, but failed to drift apart, along the margin of the Gondwana. They also attributed the early Cambrian magmatism to the extensional rifting of the crust and asthenospheric upwelling. As an alternative scenario, Ramezani and Tucker [25] using Neoproterozoic to Early Cambrian orogenic activity in an active continental margin environment. They believe geochronological and geochemical observation in

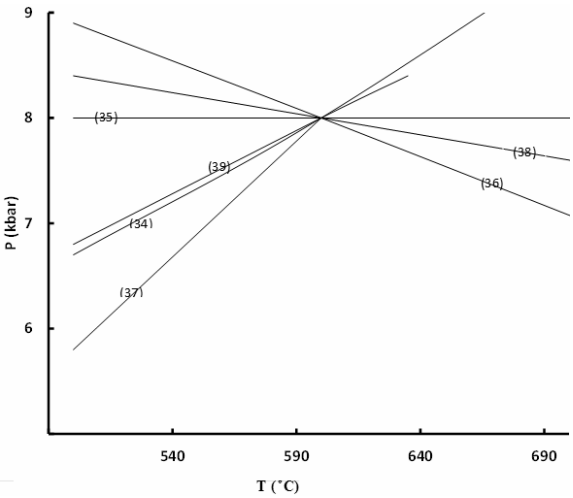

Figure 10. Cross cutting of independent reactions for M_1 assemblage.

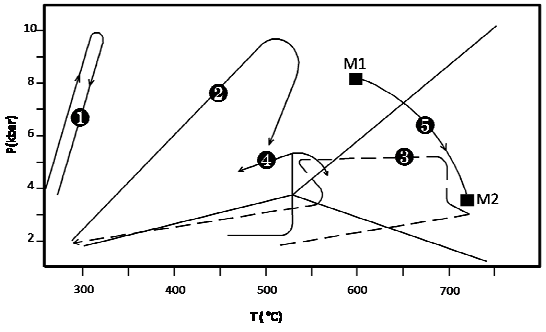

Figure 11. P-T path obtained for the studied metamorphic rocks. 1 and 2 are paths of Franciscan and Alpine type of subduction zone metamorphism (Spear [30]). 3 and 4 are P-T paths for the lower and upper plates of Acadian terrain of New England provided for comparison (Spear et al. [31]). 5 is the P-T path obtained from this study.

central Iran proposed a major episode of Latest that metamorphic complex in central Iran indicate a Late Neoproterozoic-Early Cambrian metamorphism in an orogenic setting and that the Early Cambrian granites as well as the volcanic rhyolite-dacite associations demonstrably originated in active margin environment and do not show alkaline affinities attributable to intra-plate magmatism. They also proposed that Early Cambrian evaporate facies were developed in extentional, back-arc environment [25]. This hypothesis was also supported by other researchers (e.g. [14,17]). In the subduction setting such as Japan, Turkey, the Cyclades (Greece), New Zealand [9, 10, 39] the P-T path shows a generally clockwise loop where the high pressure-low temperature subduction zone metamor-phism is followed by decompression, often with substantial heating. The metamorphic consequence of this P-T path is extensive greenschist or amphibolites facies overprint on the early blueschist and eclogite facies assemblages [10]. On the other hand, the P-T path from continental collision settings such as Acadian orogeny in central New England, U.S.A. [30], the early part of the path is nearly isobaric heating passing through the andalusite field and is interpreted to result from regional contact metamorphism. The thermal peak was followed by a period of loading followed by cooling, which is interpreted as representing the nappe stage of deformation. The path for the lower plates also shows an early low pressure part in the andalusite field followed by an increase in pressure followed by minor heating or cooling [30] (Fig. 11). Crustal temperature can also increase during lithospheric extension [22], leading to incipient rifting with or without magmatic underplating. Alkaline magmatism can itself be considered as a product of such rifting. The subsequence loading must then be an expression of shortening that immediately followed extension, with the time interval between the two processes being small enough for heat to be inherited by the compressional phase from the preceding extensional phase during tectonic regime inversion [28,12]. Such thermally softened extensional zones are vulnerable to later thickening during orogenesis [38]. It was shown in this study that Late Neoproterozoic-Early Cambrian schists in southwest of Zanjan underwent two stages of metamorphism (M_1 and M_2). The average P-T calculated for independent set of reactions and Schrinemakers' analysis for M_2 and M_1 stages of metamorphism were 5.3Kbar and 690°C and 8.5Kbar and 580°C respectively (Fig. 11). Thus, the inferred pressure-temperature path represents a clockwise P-T path from intermediate pressure Barrovian type metamorphism (M_1) towards low pressure-high

Table 5. Stable reactions (a, b, c, d) and independent set of reactions (e) obtained for M_1 assemblage containing white mica, chlorite, biotite, plagioclase, staurolite, quartz and fluid phases in the K_2O-Al_2O_3–SiO_2–MgO–FeO–Na_2O–CaO–H_2O (KNCMFASH) system. a) Stable reactions containing mu, cel, clin, phl, ann, fst, q and H_2O. b) Stable reactions containing mu, cel, clin, phl, ann, fst, q and H_2O. c) Stable reactions containing mu, clin, ames, phl, ann, east, fst, and H_2O. d) Stable reactions containing mu, clin, ames, phl, ann, east, fst and H_2O. e) Independent set of reactions for M_1 assemblage containing white mica, chlorite, biotite, plagioclase, staurolite, quartz and fluid phases

a)	
[11]	**400mu+33clin+197daph=165cel+235ann+70fst+780H_2O**
[12]	**205mu+41clin+24daph+25q=205cel+30fst+200H_2O**
[13]	**131mu+31clin+24ann+197q=155cel+18fst+88H_2O**
[14]	**20cel+9daph=5mu+4clin+15ann+35q+20H_2O**
[15]	**205cel+131daph=41clin+205ann+10fst+400q+340H_2O**
[16]	**41mu+31daph=41ann+8fst+33q+108H_2O**
b)	
[17]	**240mu+138clin+56ann=99cel+197phl+42fst+468H_2O**
[18]	**131mu+31clin+24ann+197q=155cel+18fst+88H_2O**
[20]	**4cel+clin=mu+3phl+7q+4H_2O**
[21]	**123cel+54clin+8ann=131phl+6fst+240q+204H_2O**
[22]	**123mu+93clin+32ann=155phl+24fst+99q+324H_2O**
c)	
[23]	**141mu+138clin+56ann+99east=296phl+42fst+468H_2O**
[24]	**Clin+east=ames+phl**
[25]	**141mu+296ames+56ann=158clin+197east+42fst+468H_2O**
[26]	**141mu+138ames+56ann=158phl+39east+42fst+468H_2O**
[27]	**141mu+39clin+99ames+56ann=197phl+42fst+468H_2O**
d)	
[28]	**13clin+8ann+41east+47q=49phl+6fst+40H_2O**
[29]	**39mu+62phl+6fst=8ann+93east+138q+12H_2O**
[30]	**3mu+clin+phl=4east+7q+4H2O**
[31]	**147mu+62clin+8ann=155east+6fst+296q+236H_2O**
[32]	**123mu+93clin+32ann=155phl+24fst+99q+324H_2O**
[33]	**141mu+138clin+56ann+99east=296phl+42fst+468H_2O**
e)	
[34]	**Clin+east=ames+phl**
[35]	**85mu+8daph+50plh+195q=135cel+3clin+10fst**
[36]	**85mu+27clin+50ann+195q=135cel+22daph+10fst**
[37]	**35mu+8daph+50east+195q=85cel+3clin+10fst**
[38]	**82mu+8daph+41phl+174q=123cel+10fst+12H_2O**
[39]	**94mu+8daph+47phl+12ab+192q=12pa+141cel+10fst**

temperature Buchan type metamorphism (M_2) (Fig. 11). The obtained clockwise P-T path is characteristic of the metamorphic evolution of orogenic belts whose formation involved tectonic thickening of the crust [30, 31]. The thermobarometric estimates show that the studied rocks were at a depth of 28-31 km when they experienced their peak metamorphic temperature of 561-600°C. This reflects a mean geothermal gradient of about 30°C/km that can be considered as an indicative for collision tectonics [30]. The convergence and crustal thickening implied by this intermediate pressure event was followed by low pressure-high temperature metamorphism (M2). The deduced P-T path shows that a pressure decrease of 3-4 Kbar was responsible for the retrograde P-T path since it is accompanied by an almost 100°C temperature increase. The increasing of temperature may show that exhumation was accompanied by magmatic activity such as Doran granite in the studied area. Compare with equivalent units from central Iran [30] suggests that metamorphic evolution of Late Neoproterozoic-Early Cambrian schists in southwest of Zanjan took place during the Pan-African orogeny.

Acknowledgements

The University of Zanjan supported this study; this support is gratefully acknowledged. The authors are deeply grateful to anonymous reviewer for constructive comments and English editing efforts.

References

1. Aghanabati A. Major sedimentary and structural units of Iran (map). *Geosciences*, **7**: (1998).
2. Alavi M. Tectonostratigraphic synthesis and structural style of the Alborz mountain system in northern Iran. *Journal of Geodynamics*, **21**: 1-33 (1996).
3. Alavi M., Vaziri H., Seyed-Emami K., and Lasemi Y. The Triassic and associated rocks of the Nakhlak and Aghdarband areas in central and northeastern Iran as remnants of the southern Turanian active continental margin. *Geological Society of America Bulletin*, **109**: 1563-1575 (1997).
4. Babakhani A.R., and Sadeghi A. Geological map of Zanjan. Geological Survey of Iran, Scale 1:100000 (2005).
5. Berberian M., and King G.C.P. Towards a paleogeography and tectonic evolution of Iran. *Canadian Journal of Earth Sciences*, **18**: 210-265 (1981).
6. Crawford A.R. A summary of isotopic age for Iran, Pakistan and India. *Memoire hors serie n8. Societe Geologique de France*, 251-260 (1977).
7. Davoudzadeh M., Lensh G., and Weber-Diefenback K. Stratigraphy and tectonics of the Infracambrian and Lower Paleozoic of Iran. Contribution to the Paleogeography of Iran. *Neues Jahrbuch für Geologie und Palaontologie, Abhandlungen*, **172**: 245-269 (1986).
8. Dedual E. Zur geologie des mittleren und unteren Karaj-Tales, Zentral-Elburz (Iran), *Thesis*, Mittelungen aus dem Geologischen Institut der Eidgenoessischen Technischen Hochschule und der Universitaet Zuerich, Neue Folge (1967).
9. Dempester T.J., and Tanner P.W.G. The biotite isograde, Central Pyrenees: a deformation controlled reaction. *Journal of Metamorphic Geology*, **15**: 531-584 (1997).
10. Ernst G. Tectonic history of subduction zones inferred from retrograde blueschist P-T paths. *Geology*, **16**: 1081-1084 (1988).
11. Ghavidel-Syooki M. Palynostratigraphy and palaeogeography of the Cambro-Ordovician strata in southwest of Shahrud city (Kuh-e-kharbash, near Deh-Molla), Central Alborz Range northern Iran. *Review of Paleobotany and Palynology*, **139**: 81-95 (2006).
12. Giles D., Ailléres L., Jeffries D., Betls P., and Lister G. Crustal architecture of basin inversion during the Proterozoic Isan Orogeny, Eastern Mount Isa lnlier, Australia. *Precambrian Research*, **148**: 67-84 (2006).
13. Haghipour A. Precambrian in central Iran. Lithostratigraphy, structural history and petrology. *Iranian Petroleum Institute Bulletin*, **81**: 1-17 (1981).
14. Hassanzadeh J., Stockli D.F., Horton B.K., Axen G.J., Stockli L.D., Grove M., Schmitt A.K., and Walker J.D. U-Pb zircon geochronology of Late Neoproterozoic-Early Cambrian granitoids in Iran: Implications for paleogeography, magmatism, and exhumation history of Iranian basement. *Tectonophysics*, **151**: 71-96 (2008).
15. Holland T.J.B., and Powell, R. An enlarged and updated internally consistent thermodynamic dataset with uncertainties and correlations: The system K_2O-MnO-FeO-Fe_2O_3-Al_2O_3-TiO_2-SiO_2-C-H_2-O_2. *Journal of Metamorphic Geology*, **8**: 89-124 (1990).
16. Holland T.J.B., and Powell R. An internally consistent thermodynamic data set for phases of petrological interest. *Journal of Metamorphic Geology*, **16**: 309-43 (1998).
17. Horton B.K., Hassanzadeh J., Stockli D.F., Axen G.J., Gillis R.J., Guest B., Amini A., Fakhari M.D., Zamanzadeh S.M., and Grove M. Detrital zircon provenance of Neoproterozoic to Cenozoic deposits in Iran: Implication for chronostratigraphy and collisional tectonics. *Tectonophysics,* **451**: 97-122 (2008).
18. Huckriede R., Kürsten M., and Venzlaff H. Zur geologie des gebiets zwischen Kerman und Saghand (Iran). *Beihefte zum Geologischen Jahrbuch*, **51**: 197 (1962).
19. Hushmandzadeh A. Metamorphisme et granitisation du massif Chapedony (Iran central), *Thesis*, Universite Scientifique et Medicale de Grenoble, France (1969).
20. Husseini M.I. Tectonic and depositional model of Late Precambrian-Cambrian Arabian and adjoining plates. *American Association of Petroleum Geologists Bulletin*, **73**: 1117-1131 (1989).
21. Jackson N.J., Walsh J.N., and Pegram E. Geology, geochemistry and petrogenesis of Late-Precambrian granitoids in the central Hijaz Region of the Arabian Shield. *Contribution to Mineralogy and Petrology*, **87**: 205-219 (1984).
22. Mckenzie D. Some remarks on the development of sedimentary basins. *Earth and Planetary Science letters*,

40: 25-32 (1978).
23. Müller R., and Walter R. Stratigraphy, magmatism and structure of the Precambrian-Paleozoic Taknar inlier northwest of Kashmar. *Neues Jahrbuch für Geologie und Paläontologie, Abhandlungen*, **168**: 327- 344 (1984).
24. Ramezani J. Regional Geology, geochronology and geochemistry of the igneous and metamorphic rock suites of the Saghand area, central Iran, Ph. D. *Thesis*, Washington University (1997).
25. Ramezani J., and Tucker R.D. The Saghand region, central Iran: U-Pb geochronology, petrogenesis and implications for Gnodwana tectonics. *American Journal of Science*, **303**: 622-665 (2003).
26. Samani B.A. Metallogeny of the Precambrian in Iran. *Precambrian Research*, **39**: 85-105 (1988).
27. Samani B.A., Zhuyi C., Xueto G., and Chuan T. Geology of Precambrian in central Iran: On the context of stratigraphy, magmatism and metamorphism. *Geosciences Quarterly*, **3**: 40-63 (1994).
28. Sandiford M. Mechanics of basin inversion. *Tectonophysics*, **305**: 109-120 (1999).
29. Sengör A.M.C. Tectonics of Tethysides: Orogenic Collage Development in a Collisional Setting. *Annual Review of Earth and Planetary Sciences*, **15**: 213-244 (1987).
30. Spear F.S. *Metamorphic phase equilibria and pressure-temperature-time paths*. Monograph of Mineralogical Society of America, Mineralogical Society of America, Washington, 799p. (1993).
31. Spear F.S., Hickmott D.D., and Selverstone J. Metamorphic consequences of thrust emplacement, Fall Mountain, New Hampshire, *Geological Society of America Bulletin*, **102**: 1344-1360 (1990).
32. Stampfli G.M. Tethyan oceans. In: Bozkurt E., Winchester J. A.,and Piper J. D. A.(Eds.), *Tectonics and magmatism in Turkey and surrounding area*, Geological Society of London Special Publication, 1-23 (2000).
33. Stampfli G.M., and Borel G.D. The TRANSMED transects in space and time: constraints on the Paleotectonic evolution of the Mediterranean Domain. In: Cavazza W., Roure F., Spakman W., Stampfli G.M., and Ziegler P. (Eds.), *The TRANSMED Atlas: the Mediterranean Region from Crust to Mantle*, Springer, 53-80 (2004).
34. Stöcklin J. Structural history and tectonics of Iran. a review. *American Association of Petroleum Geologists Bulletin*, **52**: 1229-1258 (1968).
35. Stöcklin J. Possible ancient continental margin in Iran. In: Burk C. A., Drake C. L. (Eds.), *The Geology of Continental Margins*, Springer, 873-887 (1974).
36. Stöcklin J., and Eftekharnezhad J. *Explanatory text of the Zanjan quadrangle map*, Geological Survey of Iran, Iran, 100p. (1969).
37. Talbot C.J., and Alavi M. The past of a future syntaxis across the Zagros, In: Alsop G. I., Blundell D. J., Davison I. (Eds.), *Salt Tectonics*, Geological Society of London Special Publication, 89-109 (1996).
38. Thompson A.B., Schulmann K., Jezek J., and Tolar V. Thermally softened continental extensional zones (arcs and rifts) as precursor to thickened orogenic belts. *Tectonophysics*, **332**: 115-141 (2001).
39. Wang G.F., Banno S., and Takeuchi K. Reactions to define the biotite isograde in the Ryoke metamorphic belt, Kii Peninsula, Japan. *Contribution to Mineralogy and Petrology*, **93**: 9-17 (1986).
40. Williams G.D. Rotation of contemporary folds into the X-direction during overthrust processes in Laksefjord, Finnmark. *Tectonophysics*, **48**: 29-40 (1978).